Bioresources and Bioprocessing

RESEARCH

Open Access

Dynamic response of *Aspergillus niger* to single pulses of glucose with high and low concentrations

Shuai Wang[1], Peng Liu[1], Wei Shu[1], Chao Li[1], Huan Li[1], Shanshan Liu[1], Jianye Xia[1*] and Henk Noorman[2]

Abstract

Microorganisms generally encounter a fluctuating environment in their natural habitat and similar conditions also happen in large-scale bioreactors. In this work, the dynamic response of intracellular and extracellular metabolites of *Aspergillus niger* was investigated after sudden exposure to high and low excess glucose concentrations in chemostats. It was found that the steady-state pathway turnover time of the carbon flux through the central carbon metabolism (CCM) was PP pathway 50 s, EMP pathway 20 s, and TCA cycle 189 s, and an upper limit for individual metabolite concentrations in the CCM was estimated. Regardless of the glucose pulse size, little changes of amino acids levels were observed except for aspartate, which showed a significant decrease. The ATP paradox, known from other organisms, was also observed in the studied *A. niger* strain. However, a different response of the NAD^+/NADH ratio to the glucose pulses was found in *A. niger* compared to previously published observations on *Penicillium chrysogenum* and *Saccharomyces cerevisiae*. These findings are valuable for better understanding *A. niger* culture performance in large-scale bioreactors.

Keywords: *Aspergillus niger*, Substrate pulse, Glucose excess, Rapid sampling, Dynamic responses, Intracellular metabolites

Introduction

Aspergillus niger is an important fungus, which is widely distributed in nature. Due to its excellent ability to secrete proteins and organic acids, *A. niger* is extensively used as an industrial workhorse for glucoamylase, glucose oxidase and citric acid production (Lu et al. 2015). In traditional industrial scale-up, the problem of poor mixing frequently leads to a decrease of product yield. In general, the fed-batch operation mode is applied in industrial fermentation for enzyme production to avoid substrate repression and accumulate more product (Sui et al. 2017). However, if the microbial substrate consumption rate is higher than its transport rate in the reactor, the zone near the feeding port will accumulate higher substrate concentrations; while further away, there is a much lower substrate concentration (Junne et al. 2010, 2011; Neubauer and Junne 2010). It has been reported in a 12 m^3 bioreactor with a fed-batch *Escherichia coli* fermentation that a substrate concentration gradient of 5~35 mg/L was formed, with peak values up to 2000 mg/L of substrate close to the feeding point (Bylund et al. 1998). In another publication, glucose concentration gradients between 4 and 41 mg/L were measured in a 22 m^3 fermentation with *Saccharomyces cerevisiae*, while simulations show levels way above 100 mg/L near the feed inlet point. Microbial cells cultured in the bioreactor travel along with the turbulent flow, and encounter the substrate "famine" and "feast" zones repeatedly and randomly (De Jonge et al. 2014). Such fluctuating environment leads to a dynamic response of the cells, and understanding the mechanisms or regulatory patterns behind this dynamic response is relevant for solving scale-up issues (Wang et al. 2015; Delvigne and Goffin 2014).

To study these responses, a substrate stimulus–response experiment based on chemostat culture can

*Correspondence: jyxia@ecust.edu.cn; jianye.xia@gmail.com
[1] State Key Laboratory of Bioreactor Engineering, East China University of Science and Technology, Shanghai 200237, China
Full list of author information is available at the end of the article

be executed. Tailored lab-scale bioreactors, called scale-down simulators, are used to mimic the fluctuating environment in the large scale as closely as possible (Neubauer and Junne 2010). Among these scale-down approaches, substrate pulse stimulation (Aboka et al. 2012) combined with rapid sampling (Zakhartsev et al. 2015) and absolute quantification of intracellular metabolite levels (Nasution et al. 2010) is very powerful. The stimulus–response experiment is implemented by imposing disturbances (e.g., high sudden concentrations of substrate, pH excursions, rapid dissolved oxygen depletion, etc.) to the cells in a metabolic steady state; then, intracellular metabolite profiles or metabolic fluxes are quantified in the period of time after the disturbance.

The response of *S. cerevisiae* to extracellular glucose pulses has been studied by Mashego et al. (2006). It was found that the intracellular ATP concentration was significantly reduced in the first 40 s after the disturbance; whereas also the total amount of ATP, ADP and AMP was decreased. Similar studies on *Penicillium chrysogenum* (Nasution et al. 2006) and *E. coli* (Taymaz-Nikerel et al. 2011) were also reported, in which it was found that the ATP level decreased in the first 50 s after glucose pulse. However, a different NAD^+/NADH ratio was reported for *E. coli* compared to *S. cerevisiae* and *P. chrysogenum*. The NAD^+/NADH ratio in *S. cerevisiae* and *P. chrysogenum* showed a downward trend (Visser et al. 2010) after the glucose pulse, while it was opposite in *E. coli* (Taymaz-Nikerel et al. 2011). These studies implied two points: (1) microorganisms respond quickly to sudden extracellular substrate concentration changes; (2) different species can show different dynamic responses to similar disturbances. Extrapolating to other species such as *A. niger*, therefore, cannot be done; hence, dynamic experiments are required. However, research on dynamic responses of *A. niger* to extracellular nutrient pulses are scarce, meaning that an in-depth analysis is needed for this important industrial workhorse.

In this work, stimulus–response experiments via administration of glucose pulses in steady-state chemostats were carried out to study the dynamic response of a glucoamylase producing *A. niger* strain. This work explores the dynamic response of extra- and intracellular metabolites of *A. niger* to sudden high or low excess glucose concentrations. With a steady-state chemostat ($\mu = 0.08\ h^{-1}$) as the reference, both concentrations of extracellular and intracellular compounds were tracked during a short period (10 min) after the pulses. Energetic and redox states of the cell after the pulse were also evaluated, and all observations were compared with published data for other species.

Materials and methods

Strain

The strain used in this study was a glucoamylase producing strain of *A. niger* kindly provided by DSM. *Pichia pastoris* (G/9KLP3) was used in the preparation of the U-^{13}C labeled internal standard [required for the IDMS method developed by Wu et al. (2005)].

Chemostat cultivation

The chemostat culture was carried out in a 5 L bioreactor (with two Rushton impellers, NCBIO, China) with working volume of 3 L, operated under following conditions: 400 rpm impeller rotating speed, 1 vvm air flow rate, auto-controlled temperature of 34 ± 0.5 °C and auto-controlled pH 4.5 (using 3 M NaOH solution as titrant). Initial batch operation was conducted before the beginning of the continuous culture. Medium for the batch culture was composed as: 10 g/L glucose·H_2O, 0.1 g/L $CaCl_2 \cdot 2H_2O$, 1 g/L $MgSO_4 \cdot 7H_2O$, 0.67 g/L EDTA, 3 g/L $(NH_4)_2SO_4$, 3 g/L KH_2PO_4, 1.5 g/L $NaH_2PO_4 \cdot H_2O$, 0.04 g/L $MnSO_4 \cdot H_2O$, 0.02 g/L $ZnCl_2$, 0.015 g/L $CuSO_4 \cdot 5H_2O$, 0.015 g/L $CoCl_2 \cdot 6H_2O$, 0.3 g/L $FeSO_4 \cdot 7H_2O$, 1 g/L defoaming agent. The chemostat started when the initial glucose was depleted at the end of the batch phase. To keep the broth volume constant during the chemostat, a level control method was applied with an effluent pipe positioned just above the broth-free surface. The dilution rate used in this work was 0.08 h^{-1}, at which the strain showed the highest specific production rate of glucoamylase. The feed medium composition other than glucose (8.5 g/L) and $(NH_4)_2SO_4$ (2.5 g/L) was the same as batch culture medium. During both the process of chemostat and the stimulus–response experiment, the off-gas composition was analyzed using a process mass spectrometer (MAX300-LG, Extrel, America). The oxygen uptake rate (OUR) and the carbon evolution rate (CER) were calculated based on the off-gas composition and the gas flow rate.

Stimulus–response experiment

For the stimulus–response experiment, 3 mL (only 0.1% of the broth volume (3 L) in the chemostat; the dilution effect by the newly added solution can be neglected) concentrated glucose solution containing either 3.00 g or 0.34 g glucose was injected into the chemostat by a sterile syringe, within 1 s. The corresponding final average glucose concentration measured in the broth was 0.90 g/L and 0.11 g/L, respectively. Thirty samples were taken in the 10 min after each pulse. Feed and effluent were stopped during this period and restarted after sampling. Extracellular and intracellular samples were collected separately from two replicate glucose pulses. The time interval between the two pulses was 8 h to minimize

the influence of the first pulse on the second one. At this time, the OUR and CER values were virtually back to the initial steady-state levels.

Rapid sampling

An in-house-made rapid sampling device was applied for the rapid sampling after the glucose pulse. The Single Chip Microcomputer technique was employed to control the opening and closure of three valves. The device was optimized so that it takes less than 1 s to sample a volume of ~ 2 mL broth.

To capture the rapid dynamic response, samples were taken more frequently at the beginning. For the pulse experiment with 3.00 g glucose injection, the sampling time points were set as follows: one sample every 15 s in the first 3 min, every 20 s in following 3 min, and every 30 s in the last 4 min. For the experiment with 0.34 g glucose injection, one sample every 10 s in the 1st min, and every 30 s for the next 9 min. Thus, 29 samples and 24 samples were taken for the 3.00 g glucose injection and 0.34 g glucose injection, respectively.

Quenching

Precooled stainless steel beads (− 40 °C) were used for quenching the extracellular sample. About 2-mL broth was sampled rapidly to a syringe containing 32 g − 40 °C steel beads (4 mm in diameter) and filtered immediately using a 0.45 μm pore size polyvinylidene fluoride (PVDF) filter (Merck Millipore Ltd.). The filtrate was collected and stored in − 80 °C fridge until further analysis.

The cold methanol method adapted from Lameiras et al. (2015) was applied for quenching the intracellular samples. About 1 mL broth was withdrawn from the tank and immediately mixed and quenched into 10 mL 40% (v/v) methanol solution precooled to − 20 °C. Sample tubes were weighted before and after sampling for accurately quantifying the amount of sample. The mixture was then vacuum filtered using 0.8 μm pore size cellulose acetate membrane. Then, the filtered cell cake was washed twice with 20 mL 40% (v/v) methanol solution precooled to − 20 °C, and the washed filtered cake was then transferred for intracellular metabolite extraction.

Intracellular metabolite extraction

The obtained filtered cake was transferred into 25 mL 75% (v/v) boiling ethanol/water solution (95 °C water bath). For absolute quantification of intracellular metabolite concentrations, 100 μL of 100% U-^{13}C-labeled cell extract (Wu et al. 2005; Liu et al. 2016) was mixed into the mixture at the same time. After 3 min, the tube containing the mixture was transferred to ice to cool down. The mixture was then filtered and the supernatant transferred to rotary evaporator (Labconco co., Rapid Vap, America) and evaporated to final volume around 600 μL. The concentrated extraction solution was then stored in − 80 °C fridge until further analysis.

Analytical procedures

The extracellular glucose concentration was measured by a glucose reagent kit (Huili biotech co., LTD, China). The glucoamylase concentration was determined by NPG method. 11.5 μL sample was mixed with 131.5 μL p-NPG substrate (prewarmed for 5 min at 37 °C, 2 g/L 4-Nitrophenyl-α-D-glucopyranoside, Sigma N-1377). After incubation at 37 °C for 20 min, the reaction was stopped by adding 57 μL 0.3 M Na_2CO_3 with immediate absorbance reading at 405 nm on a plate reader (MKIII plate reader, Thermo-Fisher, USA).

In this study, the extracellular organic acids detected are mainly oxalic acid, citric acid and pyruvate. The concentrations of extracellular organic acids were measured using HPLC, using an Agilent Technologies Hi-Plex H column (300 × 7.7 mm) equipped with a guard column (50 × 7.7 mm). The mobile phase used was 3 M H_2SO_4, with a flow rate of 0.4 L/min.

The concentrations of the glycolytic, pentose phosphate pathway and TCA cycle intermediates and the nucleotides in the cell extracts were analyzed with isotope dilution mass spectrometry (IDMS) (de Jonge et al. 2014; Suarez-Mendez et al. 2017). The intracellular metabolites concentration was measured by LC–MS/MS, using an ACQUITY UPLC BEH C18 column (1.7 μm, 2.1 mm × 150 mm) equipped with a VanGuard Pre-column (1.7 μm, 2.1 mm × 5 mm). The negative ion selected reaction monitoring (SRM) mode was used for the mass spectrometric detection. The MS data were processed using Xcalibur (V3.1.66.10, Thermo Scientific).

The intracellular amino acids concentrations were measured using GC–MS, with a HP-5MS non-polar elastic quartz capillary column (30 m × 0.25 mm × 0.25 μm). Selected ion monitoring (SIM) mode was used for accurate quantification of individual amino acids (De Jonge et al. 2011; Carnicer et al. 2012).

Results

The dynamic response of *A. niger* under two different glucose pulse concentrations was investigated. Here, the "high" or "low" concentration of glucose referred to 0.90 g/L glucose or 0.11 g/L glucose, respectively. In the stimulus experiment with the "high" glucose concentration, the cells experienced a glucose excess phase; while the cells in the stimulus with the "low" glucose concentration experienced first a glucose excess phase, followed by a glucose-depletion phase.

Metabolic fluxes and intracellular metabolite pools in steady state

Duplicate chemostat steady-state experiments with a dilution rate of 0.08 h^{-1} were carried out. The biomass concentration, oxygen consumption rate (OUR) and carbon evolution rate (CER) during the process were monitored (shown in Fig. 1). Biomass and OUR values increased exponentially during the batch phase, and decreased sharply when the batch phase finished after 16 h as the initial glucose in the broth was depleted (data not shown). Continuous feeding of fresh medium started at the end of the batch phase to implement the chemostat culture. The biomass, OUR and CER values showed no change after three residence times, and we assumed that the steady state was established after five residence times (Fig. 1). When the single pulse was carried out, the CER and OUR showed a significant increase (8.68~11.15 mmol/L/h and 8.42~10.57 mmol/L/h). With the increase of glucose concentration, the rate of glucose consumption increased, which resulted in a significant increase of CER/OUR. Exchange fluxes of individual compounds were calculated, and carbon and redox balances were both checked to make sure that all necessary compounds were taken into account (Table 1). The data reconciliation method based on a mass balance (Smolke 2010) was applied to minimize the influence of measurement errors for analyzing the steady-state data.

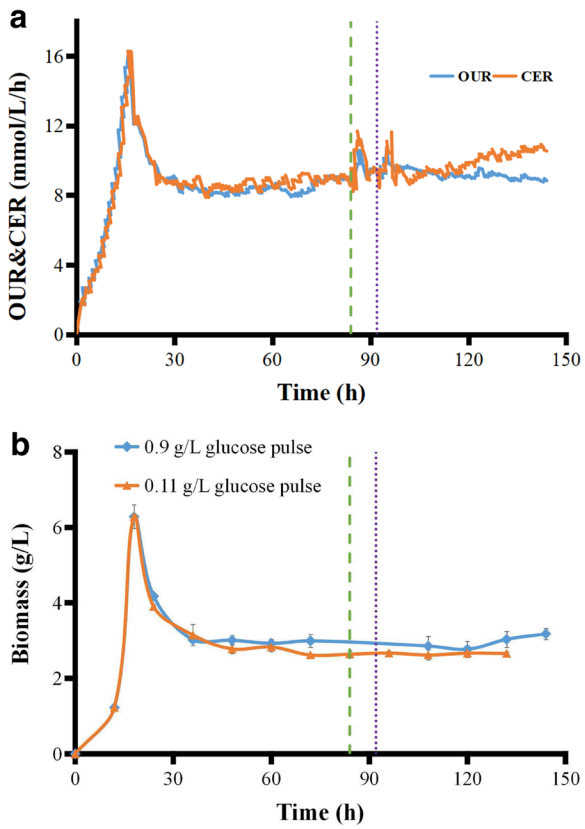

Fig. 1 **a** CER/OUR profiles over the course of the fermentation; **b** Biomass levels during the experiments. Closed lozenges are for the 0.90 g/L glucose pulse experiment and closed triangles for the 0.11 g/L glucose pulse experiment. The vertical hashed lines in the plot represent the timing of two glucose pulses, the first (green) one is for extracellular metabolites sampling and the second (purple) one for intracellular metabolites sampling

At steady state with a dilution rate of 0.08 h^{-1}, the glucoamylase concentration was 1.3 g/L. It was shown that the fungus accumulated little amount of organic acids (Table 1). The steady-state intracellular metabolite concentrations were measured as displayed in Table 2. It can be seen that steady-state levels of most intracellular metabolites are at a similar level in different organisms, which might be due to thermodynamic constraints (Heijnen 2010). However, different species and industrial strains have evolved their metabolome for specific metabolites, such as αKG and malate, which are higher in *A. niger* and *P. chrysogenum* but very low in *S. cerevisiae* and *E. coli.* The concentration of FBP in *A. niger* is obviously lower than in other species. It was found that the pools of central carbon metabolism intermediates were quite small, while the amino acids' pool sizes were much bigger. It was hypothesized that the small pool sizes of EMP, TCA and PP metabolites endowed the cell with the ability to adapt quickly to a fluctuating environment. At the same time, the relatively large pool size of amino acids ensured the cell having enough building blocks for synthesizing proteins (Heijnen 2010).

Response of extracellular metabolites

To investigate the influence of sudden glucose pulses to *A. niger* growing under glucose-limiting steady-state condition, two stimulus–response experiments with high and low glucose concentrations were conducted, respectively. Two stimuli were applied for each glucose concentration with an interval of 8 h. Extra- and intracellular metabolite samples were collected separately, i.e., one stimulus was for collecting extracellular metabolite samples, and the other

Table 1 Specific rates in steady state

Glucose — qs (g/gDW/h)	Growth μ (g/gDW/h)	GA qp (g/gDW/h)	Oxalate qOA (g/gDW/h)	Oxygen — qO_2 (g/gDW/h)	Carbon dioxide qCO_2 (g/gDW/h)	Carbon recovery (%)	Redox recovery (%)
0.23	0.08	0.03	0.04	0.08	0.11	99.31	85.96

Table 2 Intracellular metabolite concentrations in steady-state glucose-limited aerobic cultures of several organisms

Metabolites	Intracellular level (μmol/gDW)			
	A. niger ($\mu = 0.08\ h^{-1}$) [This work]	*E. coli* ($\mu = 0.1\ h^{-1}$) Taymaz-Nikerel et al. (2011)	*P. chrysogenum* ($\mu = 0.05\ h^{-1}$) Nasution et al. (2006)	*S. cerevisiae* ($\mu = 0.08\ h^{-1}$) Mashego et al. (2006) and Visser et al. (2010)
Central metabolites				
G6P	1.1	1.4	4.6	2.2
F6P	0.3	0.4	0.7	0.4
T6P	–	0.1	0.6	0.4
FBP	0.1	0.8	0.9	0.4
GAP	–	0.2	–	0.1
2PG&3PG	1.6	1.7	0.6	1.8
PEP	1.0	1.6	0.2	1.7
Pyr	1.0	0.8	0.2	0.1
Cit&Iso Cit	9.4	–	–	4.7
αKG	2.8	0.3	2.1	0.2
Suc	2.0	2.7	0.2	0.1
Fum	3.1	0.2	0.7	0.1
Mal	4.3	0.9	3.3	0.7
6PG	0.1	0.1	0.3	0.4
R5P&RL5P	2.0	–	–	–
S7P	2.3	–	–	–
E4P	0.1	–	–	–
Adenine nucleotides				
AMP	0.4	0.9	0.3	0.6
ADP	1.7	2.3	1.0	1.3
ATP	5.0	6.0	7.4	7.0

for intracellular metabolite samples. After the glucose pulse, the extracellular glucose concentration increased sharply from 0.01 to 0.90 g/L for the 3.00 g glucose pulse or 0.11 g/L for the 0.34 g glucose pulse (Fig. 2), respectively. For the extracellular residue glucose concentration changes during the first 10 min after the 0.34 g glucose pulse, three stages were observed (Fig. 2c): the steady-state phase (SS), the glucose-rich phase (phase I), and the glucose-depletion phase (phase II).

In the time window of 10 min after the glucose pulses, there was no impact on the biomass and glucoamylase levels (Fig. 3). This can be attributed to two aspects, (1) for synthesizing new functional proteins, it needs a long process including activating tRNA, translation of mRNA, folding, transferring, etc.; (2) the relatively large pool size of amino acids buffers the influence of the glucose pulse, making sure that the cell has enough building blocks for synthesizing proteins. These two aspects resulted in no significant increase or decrease of protein abundance. However, organic acids, as intermediates of the primary metabolism, are much easier influenced by the extracellular glucose fluctuation. All measured extracellular organic acids (oxalate, citrate/iso-citrate, and pyruvate) showed a clear increase (to the extent of twofold, Fig. 4). No significant difference in changes for oxalate and citrate/isocitrate were observed, regardless of the pulse glucose concentration; while it was striking that the extracellular pyruvate concentration showed a higher increase after the low glucose concentration pulse than that after the high glucose concentration pulse.

Based on the fitting data of extracellular sugar concentration, we calculated the dynamic glucose uptake rate after both glucose pulses. The glucose uptake rate of two different concentration pulse experiments is dynamically changing. The glucose uptake rate increased sharply from 0.23 to 0.53 g/gDW/h for the 0.90 g/L glucose pulse and 0.65 g/gDW/h for the 0.11 g/L glucose pulse. The glucose uptake rate after the 0.90 g/L glucose pulse dropped to 0.47 g/gDW/h in 600 s. For the 0.11 g/L glucose pulse, the glucose uptake rate quickly dropped to 0.02 g/gDW/h as the extracellular glucose concentration was depleted. Higher concentrations of glucose result in a somewhat lower glucose uptake rate. This was really interesting observations, which implied that glucose transporters with different affinities

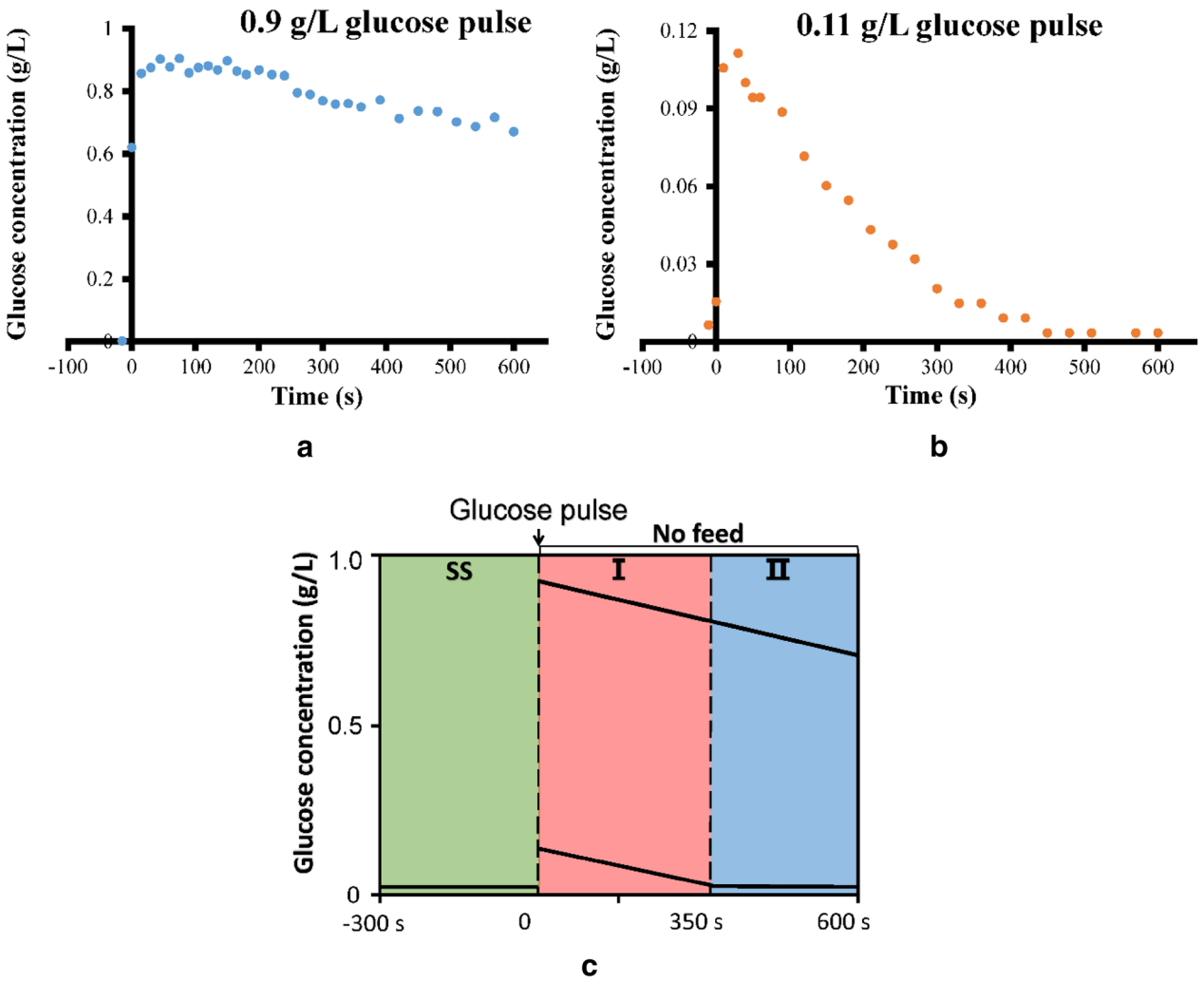

Fig. 2 Extracellular glucose concentration profiles in the first 10 min after the glucose pulses. **a** High glucose concentration (3.00 g glucose addition via a syringe containing concentrated glucose concentration); **b** low glucose concentration (0.34 g glucose); **c** phasing scheme of the glucose pulse experiments (SS: steady state; I: glucose-rich phase and II: glucose-depletion phase for the low glucose concentration pulse experiment)

(Sloothaak et al. 2015) took responsibility for the glucose uptake under different extracellular glucose concentration. This observation is also in accordance with the finding of Torres et al. (1996). They found that the low-affinity glucose transporter took control of the glucose uptake when *A. niger* was grown under high extracellular glucose condition. This may be related to different kinetic properties of the various glucose transport proteins.

Response of intracellular metabolites

The central carbon metabolism pathways

Figure 5 shows the response of metabolites in the central carbon metabolism of *A. niger* after the glucose pulses. Trehalose-6-phosphate (T6P) in the trehalose pathway has the highest intracellular response level (~20-fold). With the injection of concentrated glucose, more glucose molecules transported quickly into the cell, and entered the EMP pathway first. G6P and F6P, which are the first two metabolites, displayed a dramatic response to the extracellular glucose pulses. We calculated the steady-state pathway turnover time according to the relative flux of *A. niger* at steady state (turnover time = metabolic pool size/metabolic rate) (Lu et al. 2015). It was found that the turnover time of the carbon flux through the central carbon metabolism (CCM) was PP pathway 50 s, EMP pathway 20 s, and TCA cycle 189 s, respectively. In addition, we propose the pathway turnover time under dynamic conditions (defined as $\hat{\tau} = \frac{\sum_1^n \tau_i}{n}$ with τ_i

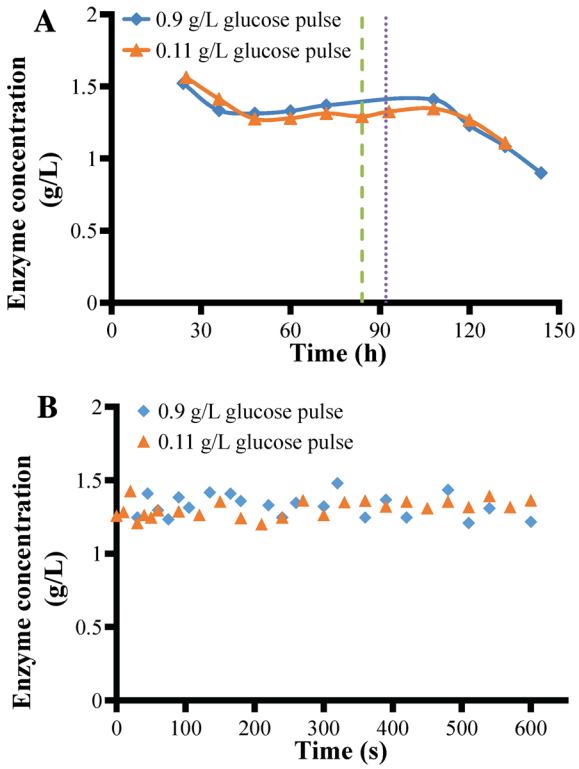

Fig. 3 **a** Profiles of the extracellular glucoamylase concentration over time; **b** extracellular glucoamylase concentrations during 10 min after the glucose pulses applied at 84 h of fermentation. Closed lozenges are for the 0.90 g/L glucose pulse experiment and closed triangles for the 0.11 g/L glucose pulse experiment. The meaning of the two vertical dashed lines is the same as Fig. 1

representing the turnover time under the *i*th time point). The pathway turnover time under dynamic conditions is used to describe the dynamic time spent for the new carbon through each entire pathway. As shown in Fig. 6, the pathway turnover time for high and low glucose pulses is almost the same, while both higher than the steady-state pathway turnover time. In particular, the pathway turnover time of the EMP and PP pathways is much higher than that of the steady state, which indicates a buffering effect of each pathway after the extracellular glucose pulses.

The amount of carbon retained in the central carbon metabolism metabolites as a function of time after the pulses is shown in Fig. 7. The accumulated glucose consumption was 161 μmol/gDW at 60 s and 404 μmol/gDW at 150 s after the high glucose pulse (0.90 g/L), while it was 179 μmol/gDW at 60 s and 388 μmol/gDW at 150 s after the low glucose pulse (0.11 g/L). In the first 60 s after pulse, 40% of the consumed glucose-embedded carbon went into the metabolite pools of the central carbon metabolism (19% to EMP, 22% to PP, and 0.01% to TCA) for the high glucose pulse (0.9 g/L), while it was 60% (20% to EMP, 34% to PP, and 6% to TCA) for the low glucose pulse. After 150 s of the pulses, there was still over 20% of consumed glucose-embedded carbons retained in central carbon metabolism metabolites. In addition, the accumulated carbons were converted into storage compounds such as trehalose or mannitol, like in *P. chrysogenum* (De Jonge et al. 2014). In the central carbon metabolism (pie chart in Fig. 7), the partial metabolite pools of the EMP and PP pathways decreased over time after the pulses, while the pool of TCA cycle intermediates increased. For high glucose stimulus, the carbon pools of the TCA cycle intermediates increased from 0.01% at 60 s to 69% at 600 s of the total glucose carbon assimilated (data not shown). Nevertheless, contrary to common sense, the carbon pool of TCA cycle responded more quickly at the low glucose pulse than at the high glucose pulse. The carbon pool of TCA intermediates increased to 9% of the assimilated glucose in 60 s, which was about three orders of magnitude higher than in steady state. This counter-intuitive phenomenon may imply that there was a repression of a specific enzymatic step at the higher glucose concentration before the glucose carbon entered the TCA cycle.

Even though there was one-order difference of the stimulus extracellular glucose concentration (0.90 g/L vs 0.11 g/L), the maximum intracellular concentration of the individual metabolites almost stayed at the same level. This indicates that there may be a threshold concentration for each metabolite, which cannot be exceeded. Estimated threshold levels for the central carbon metabolism are listed in Table 3. It is believed that they are determined by the concentration and kinetics of enzymes that are associated with these metabolites.

Most central carbon metabolism metabolites went through a short peak and then returned to their steady-state levels at the low glucose pulse. For the high glucose pulse, the peak was similar, but because the glucose levels only slowly declined also the intracellular response was slower. During this pulse, the response of 6PG followed that of G6P; a similar result that was observed in *S. cerevisiae* before (Suarezmendez et al. 2014). The response of FBP, which rose very quickly after the pulse and remained at a relatively high level, was also similar to that in *S. cerevisiae* (Mashego et al. 2006; Theobald et al. 2015). Conversely, through the low glucose pulse, 6PG and 2PG&3PG decreased slightly. FBP increased briefly after the pulse and gradually decreased to the steady-state level. The dynamic response of metabolites in the TCA cycle is quite different from those in the glycolytic and pentose phosphate pathways. Most of the metabolites in the TCA cycle were significantly elevated after the pulse (except

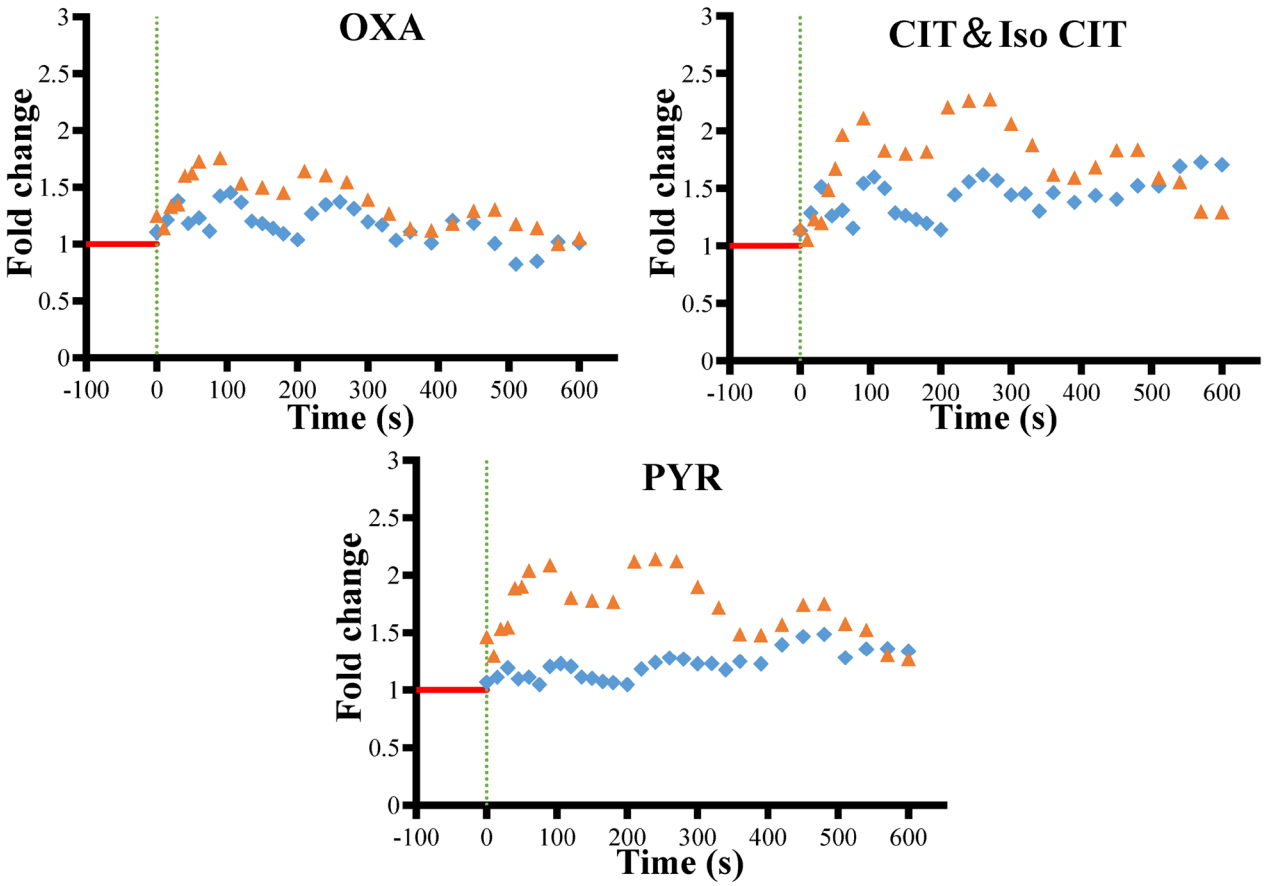

Fig. 4 Changes of extracellular organic acids during the first 10 min after the glucose pulses. Fold changes of OXA, CIT&Iso-CIT and PYR of the 0.90 g/L glucose pulse experiment (closed lozenges) and 0.11 g/L glucose pulse experiment (closed triangles). Vertical hashed lines represent the start of the glucose pulse. The steady-state level is represented as red horizontal line

the oxaloacetate concentration, which was too low to be measured) but with a longer time delay (200–400 s), which was only 100 s in the EMP and PP pathways.

In phase I after the glucose pulses (Fig. 2c), when the extracellular glucose concentrations were in excess, an almost similar response of the intracellular metabolites was observed for the two different glucose pulses (Fig. 5 and Table 4). In phase II (Fig. 2c), even though similar amounts of biomass, glucoamylase and extracellular organic acids were observed for the two different glucose pulses, there were quite different intracellular metabolites concentrations. The most obvious differences in intracellular metabolites were found for G6P, F6P, R5P&RL5P, S7P, FDP, αKG and Mal (more than twofold difference, see Table 4). To understand the metabolic regulation mechanism, a further analysis by metabolic modeling is needed (Yu and Shimizu 2015).

The intracellular amino acids

About intracellular amino acids, only slight changes (Table 5) were observed due to their relatively higher levels. Supply of precursors for these amino acids seems to play a dominant role in determining the concentration of individual amino acids. For example, αKG, precursor for Lys, Arg, Gln, Glu and Pro biosynthesis, showed a rapid ascent within 400 s after pulse, followed by the same change trend of its derived amino acids. For phase I after the glucose pulse, there seem no significant differences for the amino acids between both glucose pulses. In phase II, however, lower amino acid concentrations were observed for all amino acids after the 0.11 g/L glucose pulse due to a shortage of precursors, as the extracellular glucose became depleted. It was interesting to see that Asp showed a significant decrease but no recovery even when the glucose concentration was high in phase I. This is consistent with observations with *S. cerevisiae* under similar glucose stimulus conditions (Wu et al. 2006).

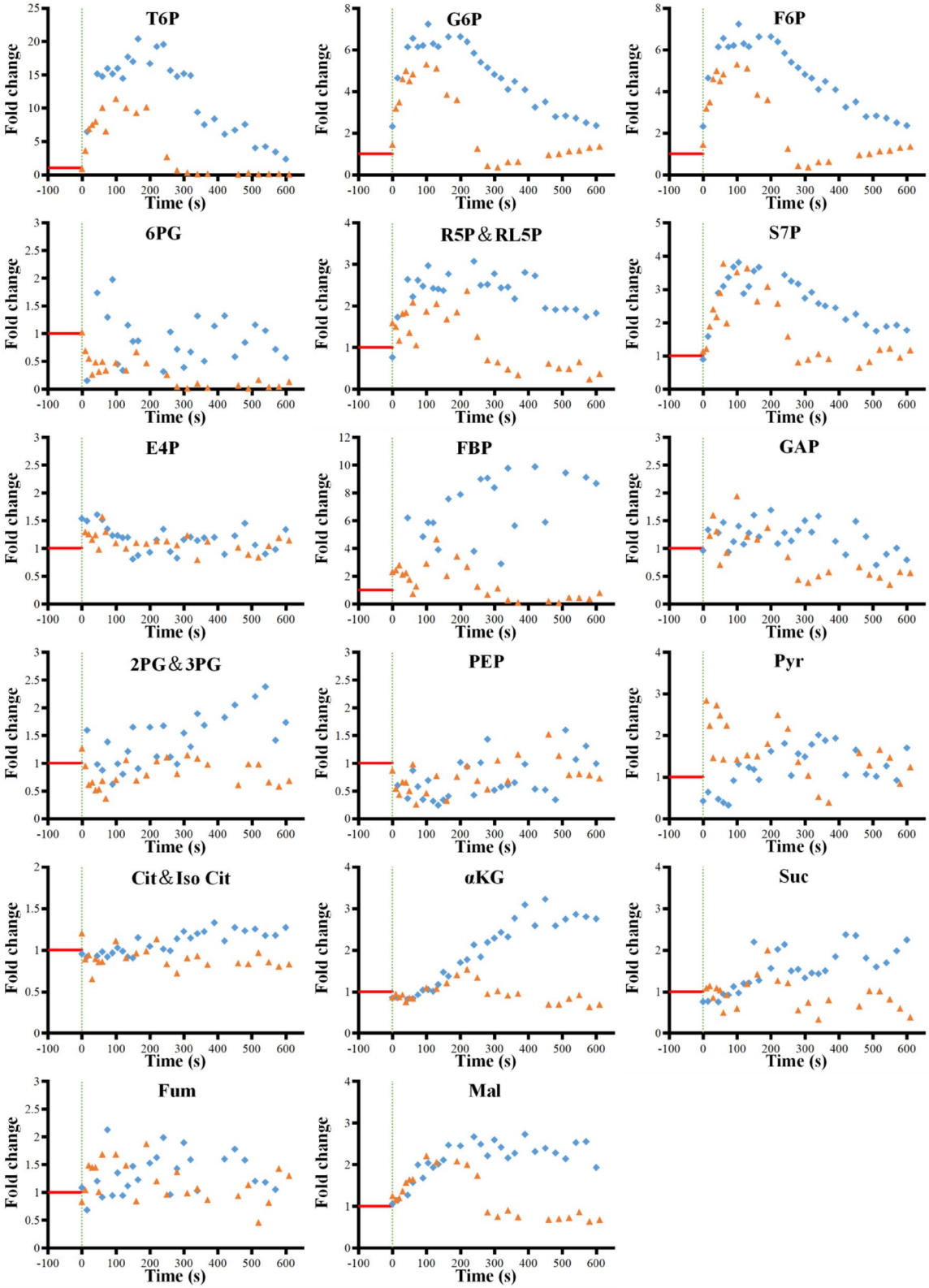

Fig. 5 Fold changes of intracellular central carbon metabolic intermediates during the first 10 min after the glucose pulses. Vertical hashed lines represent the start of the glucose pulse. The steady-state level is represented as red horizontal line

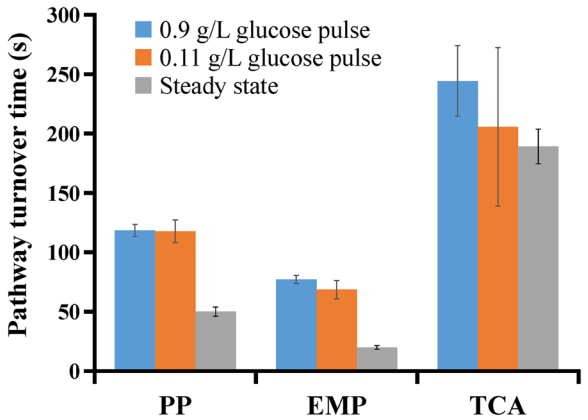

Fig. 6 Pathway turnover time in the central carbon metabolism after the glucose pulses. The bar chart shows the average turnover time for the first 10 min after the pulse of the EMP, PP, TCA pathway and the steady state

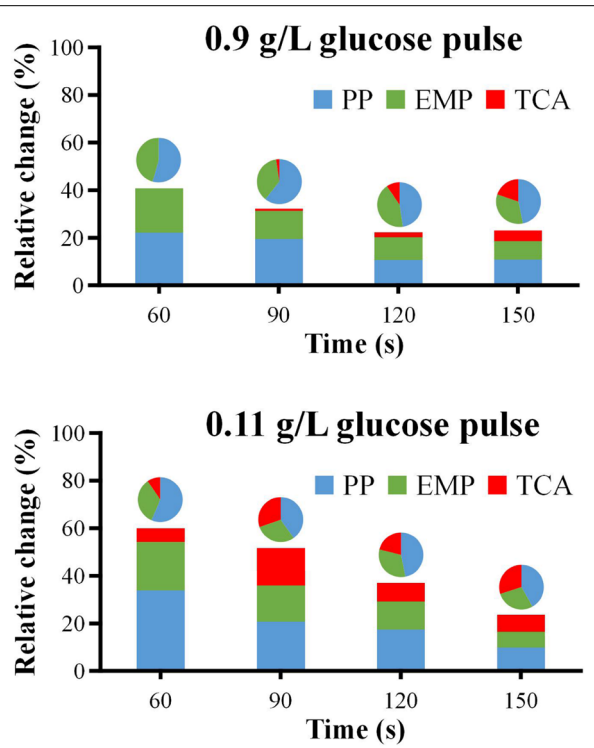

Fig. 7 Carbon accumulation in the central carbon metabolism metabolites after the pulses. The bar chart shows the relative amount of carbons accumulated in the central carbon metabolism assimilated from glucose. The pie chart above each bar shows percentages of carbons accumulated in EMP, PP, TCA pathway intermediates, respectively

The intracellular adenine nucleotide response

After the 0.90 g/L glucose pulse, the intracellular ATP concentration dropped rapidly to half of its steady-state level in 60 s, and returned slowly to its steady-state level in the following 540 s. In contrast, the intracellular AMP level increased instantly and then fell back slowly to its steady-state level. However, the intracellular ADP level kept almost unchanged. The ATP paradox, which has been reported in *S. cerevisiae* (Walther et al. 2010), thus, was also observed in this *A. niger* strain. The energy charge (EC) value showed a slow increase in the first 100 s after the glucose pulse, and maintained at a higher level afterwards (0.8–0.9, Fig. 8).

Similar results for ATP, ADP and the total adenine nucleotide pool were observed for the 0.11 g/L glucose pulse experiment. However, a lower EC value was

Table 3 Intracellular metabolite threshold values of *A. niger*

Metabolites	Threshold value (μmol/gDW)
G6P	6.1
F6P	1.5
R5P&RL5P	4.7
S7P	7.5
αKG	6.9
Mal	10.8

Table 4 Concentration fold change of intracellular metabolites in phase II

Metabolites	Concentration fold change	
	0.90 g/L	0.11 g/L
AMP	0.8	1.0
ADP	0.9	1.0
ATP	0.8	0.9
G6P	3.4	0.9
F6P	3.4	0.9
6PG	0.9	0.1
R5P&RL5P	2.2	0.5
S7P	2.2	1.0
E4P	1.1	1.0
FBP	7.7	0.4
GAP	1.1	0.5
2PG&3PG	1.8	0.9
PEP	0.8	1.0
Pyr	1.5	1.1
Cit&Iso Cit	1.2	0.9
αKG	2.7	0.8
Suc	1.8	0.7
Fum	1.4	1.0
Mal	2.3	0.7

Metabolites use average concentration fold change in phase II

Table 5 Concentration fold change of amino acids in phase I and II

Amino acid	Concentration fold change			
	Phase I		Phase II	
	0.90 g/L glucose pulse	0.11 g/L glucose pulse	0.90 g/L glucose pulse	0.11 g/L glucose pulse
Ala	1.7	1.4	1.5	0.7
Gly	2.3	1.3	1.3	0.8
Val	1.8	1.4	1.5	0.9
Leu	1.9	2.1	0.8	0.7
Ile	2.0	2.1	1.0	0.8
Pro	2.0	1.6	1.2	0.9
Met	1.3	1.5	0.8	0.9
Ser	1.3	1.4	1.0	0.7
Thr	1.2	1.4	0.9	0.7
Phe	1.6	1.5	1.0	0.9
Asp	0.3	0.3	0.5	0.6
Lys	1.3	1.3	1.1	0.8
His	1.3	3.8	0.9	0.9
Tyr	1.6	1.8	0.9	0.9
Glu	–	1.1	–	0.8
Gln	–	1.2	–	0.8
Orn	–	1.2	–	1.0
Asn	–	1.4	–	0.8
Cys	–	1.4	–	0.9

Maximum or minimum concentration fold changes in phase I; Metabolites in phase II use average concentration fold change

observed for the lower glucose concentration, which indicated a lower energy state as less glucose was supplied. In addition, no initial increase of AMP was observed.

Comparison with similar pulse experiments in *E. coli*, *P. chrysogenum*, and *S. cerevisiae*

The metabolic response of *A. niger* to extracellular glucose disturbances was compared with that of *E. coli* (Taymaz-Nikerel et al. 2011), *P. chrysogenum* (Nasution et al. 2006) and *S. cerevisiae* (Mashego et al. 2006) in similar glucose stimulus experiments. The residual glucose concentrations after the pulses applied in this work were 0.90 g/L and 0.11 g/L, while it was 0.5 g/L for experiments carried out with *E. coli*, *P. chrysogenum* and *S. cerevisiae*. For easy comparison, fold change of metabolites concentrations after the glucose pulses was used, and the data are summarized in Table 6.

It can be observed that changes of most metabolites of the central carbon metabolism pathways showed similar trends. Note that changes listed in Table 6 only showed the maximum fold change level of the individual metabolites. Profiles of most metabolites showed almost the same patterns; however, the time when these metabolites reach their peak value was quite different among the four different species. For example, the TCA cycle intermediates took 40–60 s for *E. coli* to reach their peak values, ~100 s for *S. cerevisiae* and *P. chrysogenum*, but 200–400 s was needed for *A. niger*. According to Atkinson (Ramaiah et al. 1964), an increased glucose metabolism

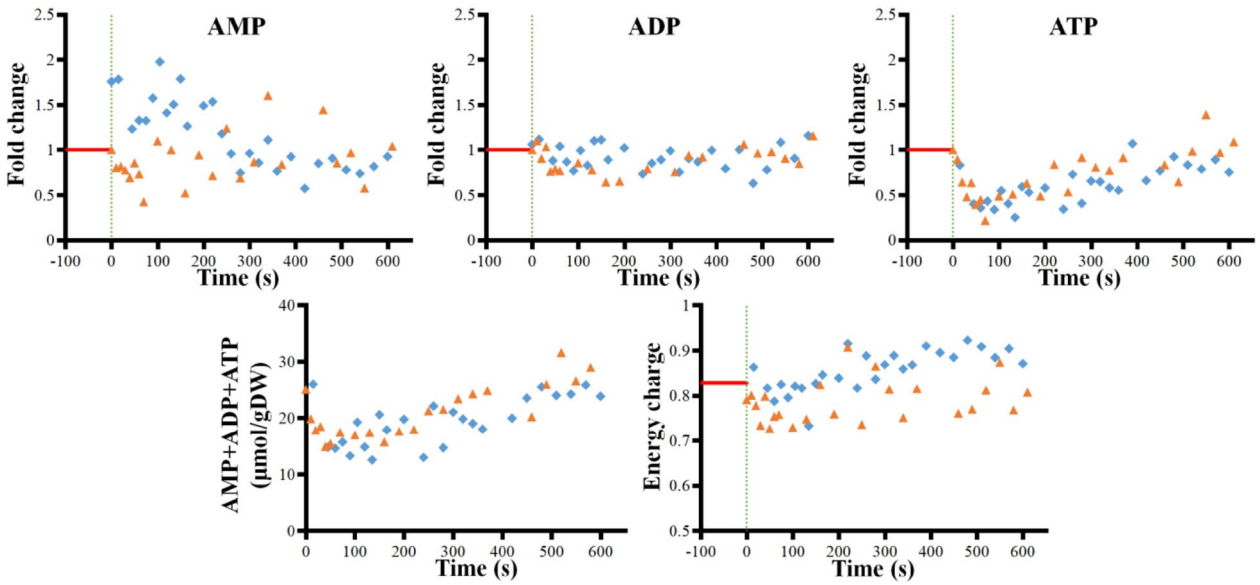

Fig. 8 Changes of nucleotides in the first 10 min after the glucose pulses. Fold change of AMP, ADP and ATP of the 0.90 g/L glucose pulse experiment (closed lozenges) and the 0.11 g/L glucose pulse experiment (closed triangles). Vertical hashed lines represent the start of the glucose pulse. The steady-state level is represented as red horizontal line

Table 6 Concentration fold change of central metabolite levels in different species

Central metabolites	Concentration fold change				
	A. niger **[This work]**	***A. niger*** **[This work]**	***E. coli*** **Taymaz-Nikerel et al. (2011)**	***P. chrysogenum*** **Nasution et al. (2006)**	***S. cerevisiae*** **Mashego et al. (2006) and Visser et al. (2010)**
	0.90 g/L	**0.11 g/L**	**0.5 g/L**	**0.5 g/L**	**0.5 g/L**
EMP					
G6P	7.2	5.3	4.8	1.9	5.2
F6P	7.2	5.3	–	2.0	5.5
FBP	9.9	4.7	–	9.3	22.0
GAP	1.7	1.9	1.1	2.0	4.1
2PG&3PG	2.4	0.4	0.3	0.1	0.7
PEP	0.2	0.3	0.1	0.1	0.5
Pyr	2.4	2.8	1.3	1.8	5.0
TCA					
Cit&Iso Cit	1.3	1.2	1.3	1.1	1.1
αKG	2.6	1.5	1.5	1.1	3.9
Suc	1.6	2.0	3.6	2.7	3.6
Fum	2.0	1.9	1.8	2.8	3.5
Mal	3.0	2.2	1.5	2.4	3.6
PP					
6PG	0.2	0.01	9.5	–	–
R5P&RL5P	3.7	2.4	–	–	–
S7P	3.8	3.8	–	–	–
E4P	1.6	2.3	4.3	–	–

Metabolites in the state of glucose excess use maximum or minimum concentration fold change

should boost both catabolic and anabolic fluxes, which needed a higher ATP/ADP level; however, this was not always the case. The ATP paradox was confirmed for all the eukaryotic cells (*S. cerevisiae* from Wu et al. (2006), *P. chrysogenum* from Nasution et al. (2006) and *A. niger* in this study). However, this was not observed in *E. coli* (Taymaz-Nikerel et al. 2011)—instead, this bacterium kept its ATP level high.

A steep increase of the NAD^+/NADH ratio immediately after the pulse was observed in *A. niger* with both high and low glucose pulses (Fig. 9a). A quick decrease, however, followed with the ratio dropping to a specific level above (for higher glucose concentration stimulus) or below (for lower glucose stimulus) the reference steady-state level. Contrasting results were reported in *P. chrysogenum* (Nasution et al. 2006) or *S. cerevisiae* (Wu et al. 2006), where the NAD^+/NADH ratio decreased after the pulse. Similar changes of the NAD^+/NADH ratio were found in *E. coli* (Taymaz-Nikerel et al. 2011) with short-time glucose pulses. This may be attributed to a highly efficient electron transfer chain system in *A. niger*. There are known three modes of operation of the ETC in *A. niger* that allow a flexible regulation of the P/O ratio to dispose excess mitochondrial NADH produced during glucose pulse. In addition, the sharp decrease of more oxidized aspartate molecule levels accompanied by a quick increase of more reduced malate molecule levels may also contribute to the accumulation of the more oxidized NAD^+.

Conclusions

To the best of our knowledge, this is the first report about the response of *A. niger*, growing under glucose-limited chemostat steady-state conditions to extracellular glucose stimuli. Two levels of glucose were used to stimulate the *A. niger* metabolism. No obvious influence on biomass or the product (glucoamylase) was observed in the short time window following the glucose stimulus. However, a slight increase of secretion of organic acid byproducts was observed.

A quick response of the central carbon metabolism intermediates was observed to both levels of glucose pulse. The steady-state pathway turnover time of glucose through the central carbon metabolism for *A. niger* was estimated to be PP pathway 50 s, EMP pathway 20 s, and TCA cycle 189 s, and the dynamic pathway turnover time

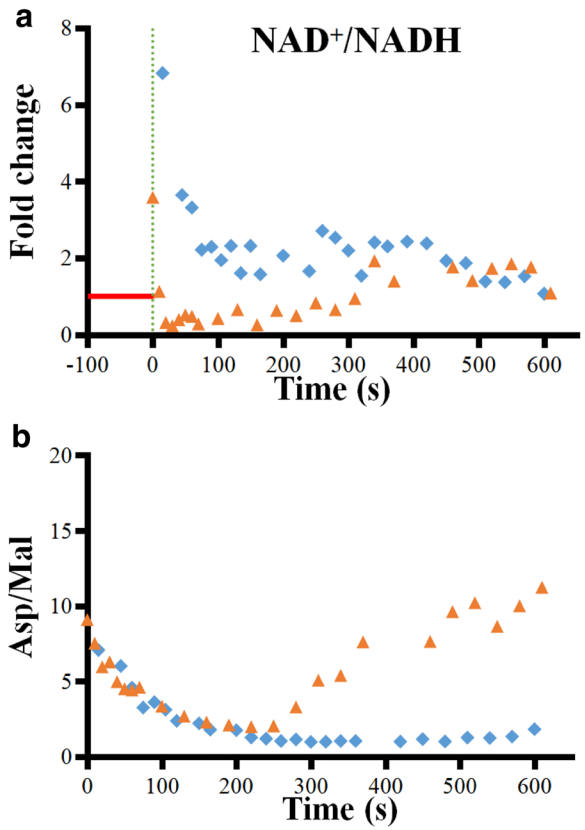

Fig. 9 **a** $(NAD^+/NADH)/(NAD_0^+/NADH_0)$ ratio profiles after the glucose pulses; **b** Asp/Mal ratio's in both glucose pulse experiments. Vertical hashed lines represent the start of the glucose pulse. The steady-state level is represented as red horizontal line

was much higher than the steady state. More than 23% of the assimilated glucose carbon retained in the central carbon metabolism pathway in a time window of 150 s. The maximum pool size of individual central carbon metabolism metabolites was estimated, and among them Mal (the threshold value to be about 10.8 μmol/gDW) and S7P (the threshold value to be about 7.5 μmol/gDW) took the first two ranks. The biggest difference between the two distinct pulses was whether the microbes entered a state of glucose depletion or not.

In the time window of 600 s, intracellular amino acid concentrations showed a slight increase except for aspartate, showing a significant decrease (to 1/3 of its reference steady-state level) regardless of the feed glucose concentration. A corresponding increase of malate and a decrease of NAD^+/NADH ratio might indicate the activation of the aspartate–malate shuttle pathway to balance cytosolic and mitochondrial NADH levels in the dynamic environment.

Discussion

The ATP paradox after a glucose pulse, reported in *P. chrysogenum* and *S. cerevisiae*, was also observed in the studied *A. niger* strain. EC value correlated well with the extracellular glucose abundance, where a higher glucose concentration gave a higher EC level. Comparison among prokaryote (*E. coli*) and eukaryotes (*S. cerevisiae*, *P. chrysogenum* and *A. niger*) showed very similar response patterns for the central carbon metabolism intermediates. However, response times and response levels were observed to be species dependent. This is obviously caused by different enzymatic activities and kinetic properties such as the affinity constants of individual metabolic reactions among different species, and cannot be extrapolated from results with other species. Another limitation to be noted is the question how relevant the response after single pulses is for large-scale operation, where the cells are exposed to continuous changes during the full process duration. It has been shown before (De Jonge et al. 2014; Tang et al. 2017; Wang et al. 2017, 2018) that under such conditions, the average metabolic state can be very different from the steady-state chemostat conditions. Further work, therefore, should concentrate on clarifying the impact of continuous dynamics on the metabolic response.

Abbreviations

AMP: adenosine-monophosphate; ADP: adenosine-diphosphate; ATP: adenosine-triphosphate; T6P: trehalose-6-phosphate; G6P: glucose-6-phosphate; F6P: fructose-6-phosphate; 6PG: 6-phosphogluconate; R5P&RL5P: D-ribulose-5-phosphate and L-ribulose-5-phosphate; S7P: sedoheptulose-7-phosphate; E4P: erythrose-4-phosphate; FBP: fructose-1,6-bisphosphate; GAP: glyceraldehyde-3-phosphate; 2PG&3PG: 2-phosphoglycerate and 3-phosphoglycerate; PEP: phosphoenolpyruvate; Pyr: pyruvate; Cit&Iso Cit: citrate and iso-citrate; αKG: α-ketoglutarate; Suc: succinate; Fum: fumarate; Mal: L-malate; Lys: lysine; Arg: arginine; Glu: glutamic acid; Gln: glutamine; Pro: proline; Asp: aspartic acid; OXA: oxalic acid; DO: dissolved oxygen; OUR: oxygen uptake rate; CER: carbon evolution rate; CCM: central carbon metabolism; EMP: Embden–Meyerhof–Parnas; TCA: tricarboxylic acid; PP: pentose phosphate; *A. niger*: *Aspergillus niger*; *E. coli*: *Escherichia coli*; *S. cerevisiae*: *Saccharomyces cerevisiae*; *P. chrysogenum*: *Penicillium chrysogenum*; IDMS: isotope dilution mass spectrometry.

Acknowledgements

Not applicable.

Authors' contributions

PL analyzed and interpreted the change of the ATP paradox and the NAD^+/NADH ratio. WS and CL designed and implemented U-^{13}C labeled cell extracts. HL and SL extracted the intracellular metabolites. SW and JX were major contributors in writing the manuscript. HN modified the pathway turnover time and polished this paper. All authors read and approved the final manuscript.

Funding

This work was supported by the National Natural Science Foundation of China [Grant Numbers 21506052, 21776082]; and the Fundamental Research Funds for the Central Universities [Grant Number 22221818014]; and the 111 Project [Grant Number B18022].

Availability of data and materials
The datasets used and/or analyzed during the current study are available from the corresponding author on reasonable request.

Ethics approval and consent to participate
Not applicable.

Consent for publication
Not applicable.

Competing interests
The authors declare that they have no competing interests.

Author details
[1] State Key Laboratory of Bioreactor Engineering, East China University of Science and Technology, Shanghai 200237, China. [2] DSM Biotechnology Center, P.O. Box1, 2600MA Delft, The Netherlands.

Received: 10 March 2019 Accepted: 4 May 2019
Published online: 21 May 2019

References

Aboka FO et al (2012) Identification of informative metabolic responses using a minibioreactor: a small step change in the glucose supply rate creates a large metabolic response in *Saccharomyces cerevisiae*. Yeast 29(3–4):95–110
Bylund F et al (1998) Substrate gradient formation in the large-scale bioreactor lowers cell yield and increases by-product formation. Bioprocess Eng 18(3):171–180
Carnicer M et al (2012) Development of quantitative metabolomics for *Pichia pastoris*. Metabolomics 8(2):284–298
De Jonge LP et al (2011) Scale-down of penicillin production in *Penicillium chrysogenum*. Biotechnol J 6(8):944–958
De Jonge L et al (2014) Flux response of glycolysis and storage metabolism during rapid feast/famine conditions in *Penicillium chrysogenum* using dynamic (13)C labeling. Biotechnol J 9(3):372–385
Delvigne F, Goffin P (2014) Microbial heterogeneity affects bioprocess robustness: dynamic single-cell analysis contributes to understanding of microbial populations. Biotechnol J 9(1):61–72
Heijnen JJ (2010) Impact of thermodynamic principles in systems biology. Adv Biochem Eng Biotechnol 121:139
Junne S et al (2010) Scale down simulator for studying the impact of industrial scale inhomogeneities on *Bacillus subtilis* processes. J Biotechnol 150(6):420
Junne S et al (2011) A two-compartment bioreactor system made of commercial parts for bioprocess scale-down studies: impact of oscillations on *Bacillus subtilis* fed-batch cultivations. Biotechnol J 6(8):1009–1017
Lameiras F, Heijnen JJ, Gulik WMV (2015) Development of tools for quantitative intracellular metabolomics of *Aspergillus niger* chemostat cultures. Metabolomics 11(5):1253–1264
Liu P et al (2016) Combined ^{13}C-assisted metabolomics and metabolic flux analysis reveals the impacts of glutamate on the central metabolism of high β-galactosidase-producing *Pichia pastoris*. Bioresour Bioprocess 3(1):47
Lu H et al (2015) Integrated isotope-assisted metabolomics and ^{13}C metabolic flux analysis reveals metabolic flux redistribution for high glucoamylase production by *Aspergillus niger*. Microb Cell Fact 14(1):147
Mashego MR et al (2006) In vivo kinetics with rapid perturbation experiments in *Saccharomyces cerevisiae* using a second-generation BioScope. Metab Eng 8(4):370–383
Nasution U et al (2006) Generating short-term kinetic responses of primary metabolism of *Penicillium chrysogenum* through glucose perturbation in the bioscope mini reactor. Metab Eng 8(5):395–405
Nasution U et al (2010) Measurement of intracellular metabolites of primary metabolism and adenine nucleotides in chemostat cultivated *Penicillium chrysogenum*. Biotechnol Bioeng 94(1):159–166
Neubauer P, Junne S (2010) Scale-down simulators for metabolic analysis of large-scale bioprocesses. Curr Opin Biotechnol 21(1):114–121
Ramaiah A, Hathaway JA, Atkinson DE (1964) Adenylate as a metabolic regulator. Effect on *Yeast* phosphofructokinase kinetics. J Biol Chem 239(239):3619
Sloothaak J et al (2015) *Aspergillus niger* membrane-associated proteome analysis for the identification of glucose transporters. Biotechnol Biofuels 8:150
Smolke C (2010) The metabolic pathway engineering handbook: fundamentals. CRC Press/Taylor & Francis, Boca Raton
Suarez-Mendez CA et al (2014) Fast "feast/famine" cycles for studying microbial physiology under dynamic conditions: a case study with *Saccharomyces cerevisiae*. Metabolites 4(2):347
Suarez-Mendez CA, Ras C, Wahl SA (2017) Metabolic adjustment upon repetitive substrate perturbations using dynamic 13C-tracing in yeast. Microb Cell Fact 16(1):161
Sui YF et al (2017) Global transcriptional response of *Aspergillus niger* in the process of glucoamylase fermentation. Bioresour Bioprocess 4(1):44
Tang W et al (2017) A 9-pool metabolic structured kinetic model describing days to seconds dynamics of growth and product formation by *Penicillium chrysogenum*. Biotechnol Bioeng 114(8):1733
Taymaz-Nikerel H, van Gulik WM, Heijnen JJ (2011) *Escherichia coli* responds with a rapid and large change in growth rate upon a shift from glucose-limited to glucose-excess conditions. Metab Eng 13(3):307–318
Theobald U et al (2015) In vivo analysis of metabolic dynamics in *Saccharomyces cerevisiae*: I. Experimental observations. Biotechnol Bioeng 55(2):305–316
Torres NV et al (1996) Glucose transport by *Aspergillus niger*: the low-affinity carrier is only formed during growth on high glucose concentrations. Appl Microbiol Biotechnol 44(6):790–794
Visser D et al (2010) Analysis of in vivo kinetics of glycolysis in aerobic *Saccharomyces cerevisiae* by application of glucose and ethanol pulses. Biotechnol Bioeng 88(2):157–167
Walther T et al (2010) Control of ATP homeostasis during the respiro-fermentative transition in *Yeast*. Mol Syst Biol 6(1):344
Wang G et al (2015) Integration of microbial kinetics and fluid dynamics toward model-driven scale-up of industrial bioprocesses. Eng Life Sci 15(1):20–29
Wang G et al (2017) Power input effects on degeneration in prolonged penicillin chemostat cultures: a systems analysis at flux, residual glucose, metabolite and transcript levels. Biotechnol Bioeng 115(1):114–125
Wang G et al (2018) Comparative performance of different scale-down simulators of substrate gradients in *Penicillium chrysogenum* cultures: the need of a biological systems response analysis. Microb Biotechnol 11(3):486–497
Wu L et al (2005) Quantitative analysis of the microbial metabolome by isotope dilution mass spectrometry using uniformly 13C-labeled cell extracts as internal standards. Anal Biochem 336(2):164–171
Wu L et al (2006) Short-term metabolome dynamics and carbon, electron, and ATP balances in chemostat-grown *Saccharomyces cerevisiae* CEN.PK 113-7D following a glucose pulse. Appl Environ Microbiol 72(5):3566
Yu M, Shimizu K (2015) Current status and future perspectives of kinetic modeling for the cell metabolism with incorporation of the metabolic regulation mechanism. Bioresour Bioprocess 2(1):1–19
Zakhartsev M et al (2015) Fast sampling for quantitative microbial metabolomics: new aspects on cold methanol quenching: metabolite co-precipitation. Metabolomics 11(2):286–301

Publisher's Note